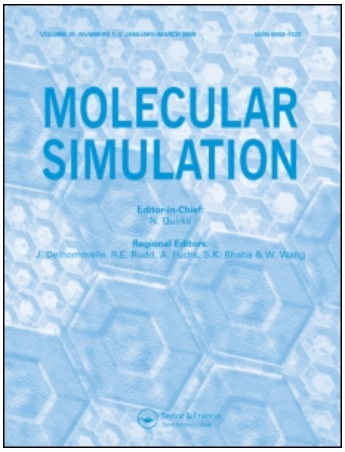

Molecular Simulation
Publication details, including instructions for authors and subscription information:
http://www.informaworld.com/smpp/title~content=t713644482

Molecular dynamics simulation on the dissociation process of methane hydrates

L. Y. Ding[ab]; C. Y. Geng[b]; Y. H. Zhao[a]; H. Wen[a]
[a] Multi-phase Reaction Laboratory, Institute of Process Engineering, Chinese Academy of Sciences, Beijing, People's Republic of China [b] Graduate University of Chinese Academy of Sciences, Beijing, People's Republic of China

To cite this Article Ding, L. Y. , Geng, C. Y. , Zhao, Y. H. and Wen, H.(2007) 'Molecular dynamics simulation on the dissociation process of methane hydrates', Molecular Simulation, 33: 12, 1005 — 1016
To link to this Article: DOI: 10.1080/08927020701528524
URL: http://dx.doi.org/10.1080/08927020701528524

Molecular Simulation, Vol. 33, No. 12, October 2007, 1005–1016

Taylor & Francis
Taylor & Francis Group

Molecular dynamics simulation on the dissociation process of methane hydrates

L. Y. DING†‡, C. Y. GENG†‡, Y. H. ZHAO† and H. WEN†*

†Multi-phase Reaction Laboratory, Institute of Process Engineering, Chinese Academy of Sciences, Beijing 100080, People's Republic of China
‡Graduate University of Chinese Academy of Sciences, Beijing 100049, People's Republic of China

(Received January 2007; in final form June 2007)

The dissociation process of methane hydrate is simulated at $P = 30$ bar and $T = 315$, 320 and 325 K, using *NPT* molecular dynamics (MD) method. An eight unit-cell methane hydrate is employed as a model system. A series of analytical results concerned with the dissociation process are used to exhibit the continuous changes of methane hydrate from crystal to liquid. As a result, the dissociation of methane hydrate is considered to be comprised of two successive stages. The first stage is the process associated with the diffusive behaviour of host molecules, which gradually leads to the increase of the cell size and ultimately results in the fracture of the lattice structure. Methane molecules will escape from the broken hydrate cavities and aggregate together in the second stage. The fracture of the lattice structure is found to be the key for hydrate dissociation.

Keywords: Clathrate hydrate; Methane hydrate; Dissociation; Molecular dynamics

1. Introduction

Gas hydrates belong to a class of nonstoichiometric ice-like inclusion clathrates, in which water molecules (host molecules) form hydrogen-bonded lattice network with gas molecules (guest molecules) encaged within the lattice cavities. Guest molecules interact with the host molecules through van der Waals' interactions. It is known that type I, II and H are the major crystal structures of gas hydrates, depending principally on the molecular size of guest molecules. Details about the structures and properties of gas hydrates are described in Sloan's reviews [1].

Gas hydrates can form during the gas/oil transportation where they pose a major problem by plugging the transportation pipelines [2]. Such hydrate formation is a nuisance, but it could also prove useful in that natural gas hydrates stored in permafrost region and beneath the sea floor play an important role as a great reserve of carbon in the world [3]. They are expected as potential future resources. In addition, gas hydrates are also drawing attention because they can be used as a gas storage medium with a high gas storage capacity [4–6].

Since the first discovery that water forms clathrate hydrate with chloride in 1810 by Sir Humphrey Davy, about 200 years of research has been devoted to understanding hydrate phenomenon. This continuous effort has well-established the thermodynamic, physical, and structural properties of gas hydrates. In contrast to the advances made in thermodynamics, the kinetics associated with formation and dissociation process is less understood [7,8]. Recently, the importance of kinetic studies on the formation and dissociation processes has been increasingly recognised. On one hand, practical and feasible hydrate exploitation technology could only be developed if hydrate dissociation kinetics are well understood. On the other hand, a good knowledge of the hydrate formation kinetics is important for designing kinetic inhibitors or anti-agglomerant hydrate inhibitors that are expected to intervene with the hydrate formation process in pipelines.

In order to achieve a thorough understanding of the formation and dissociation kinetics, it is essential to study the mechanism associated with hydrate formation and dissociation process [9,10]. However, there is still limited information about the formation and dissociation of methane hydrate at the microscopic level up to now. Molecular-scale knowledge is important to understand the molecular nature and to gain valuable insights on the mechanism of hydrate formation and dissociation process. Ota *et al.* [11] performed molecular dynamics (MD) simulation on the nucleation process of one unit cell

*Corresponding author. Tel.: +8610-62626704. Email: hwen@home.ipe.ac.cn

Molecular Simulation
ISSN 0892-7022 print/ISSN 1029-0435 online © 2007 Taylor & Francis
http://www.tandf.co.uk/journals
DOI: 10.1080/08927020701528524

methane hydrate and presented a three-step nucleation mechanism. In the first stage of nucleation, methane molecules disperse in water, water molecules form clathrate-like cavities around methane molecules in the second stage and stable hydrate structures form in the third stage. Moon *et al.* [12] simulated the methane/water interface and observed the formation of nuclei and sustained growth process. It was found that the hydrogen bonding network formed at the initial nucleation stage is dominated by pentagonal rings of water molecules rather than clathrate-like cages.

The purpose of this work is to simulate the microscopic dissociation process and discuss the likely mechanism at molecular level by performing MD simulations on type I methane hydrates under isothermal and isobaric conditions.

2. Simulation details

Methane hydrate of type I is modeled, consisted of 368 water molecules and 64 methane molecules, in a simulation box of 2 × 2 × 2 unit cell as shown in figure 1. Here, methane molecules are displayed as spheres, water molecules as lines, and hydrogen bonds as dashed lines. The initial positions of the oxygen atoms in hydrate lattice are obtained from X-ray diffraction experiment [13] and the hydrogen atoms are then added in a random manner but consistent with Bernal–Fowler rule [14]. All cavities in hydrates are assumed to be occupied by methane molecules and carbon atoms in methane molecules are placed at the centre of the cavities.

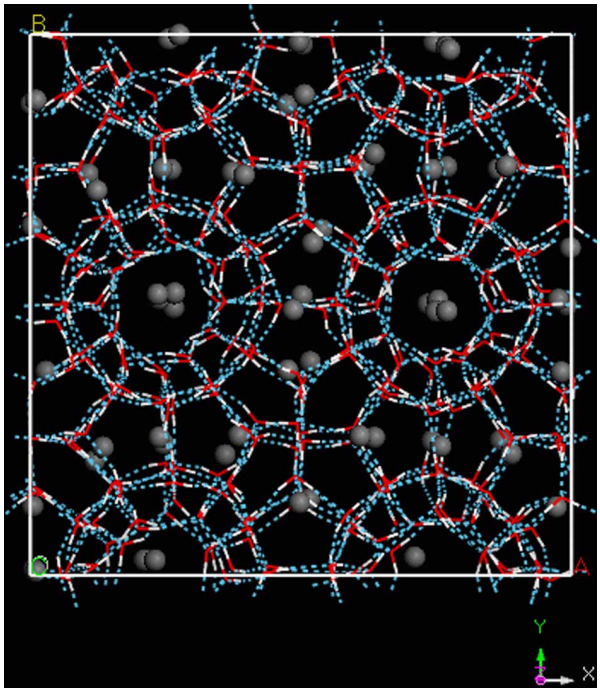

Figure 1. The simulation system of methane hydrate.

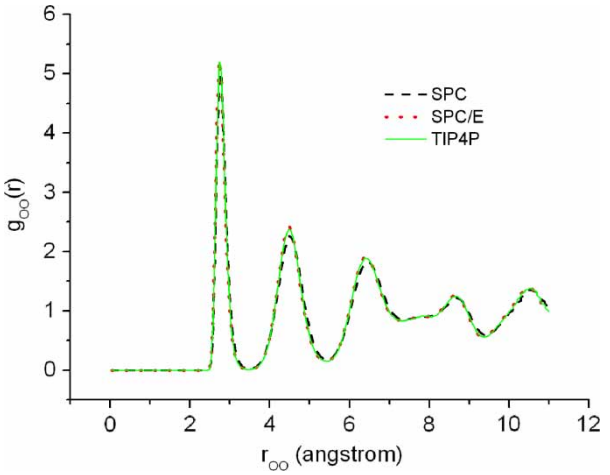

Figure 2. The RDF of oxygen atoms for three different potential models.

In order to investigate the effects of different potential models on the resulting properties of methane hydrate, Some researchers have tested a series of different models in their simulation study [15–18]. Chialvo and Cummings compared SPC, SPC/E and TIP5P model for water and OPLS and Williams model for methane. As a result, all these potential models present similar results. We have also examined SPC, SPC/E and TIP4P for water molecules in a relatively short MD simulation of 30 ps with 10 ps for equilibration. The microstructure of the hydrate is described by the site–site radial distribution functions (RDF) for the oxygen and carbon atoms. Figures 2–3 show the calculated RDF $g_{oo}(r)$ and $g_{oc}(r)$ where O and C refer to the oxygen atom in water and carbon atom in methane, respectively. It is apparent that the three models yield broadly similar results. In this study, we choose the SPC model because it is computationally less expensive.

The rigid, three-centre SPC potential model proposed by Berendsen [19] is used for water–water interactions, in which a Lennard–Jones interaction is employed for each

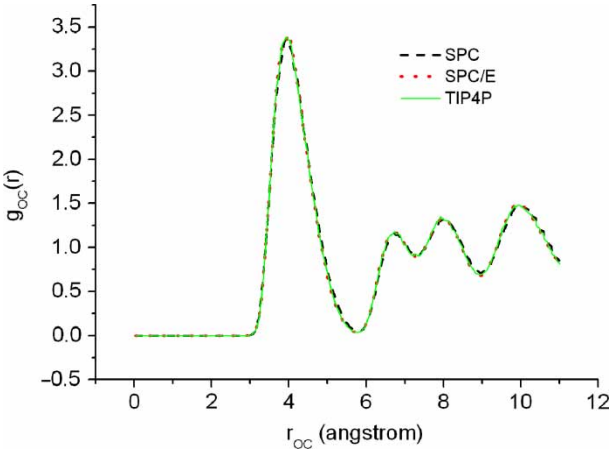

Figure 3. The RDF between oxygen and carbon atoms for three different potential models.

Table 1. Lennard–Jones parameters used in this work.

	σ (Å)	ε (kJ mol^{-1})
H_2O	3.166	0.65
CH_4	3.73	1.23

pair of oxygen sites. The potential is expressed as

$$u(r_{ij}) = \frac{q_i q_j}{4\pi\varepsilon_0 \cdot r_{ij}} + 4\varepsilon\left[\left(\frac{\sigma}{r_{ij}}\right)^{12} - \left(\frac{\sigma}{r_{ij}}\right)^{6}\right], \qquad (1)$$

where, r_{ij} is the distance between molecules i and j, q_i refers to the charges on molecule i, ε_0 is the permittivity of free space, σ and ε are the Lennard–Jones parameters. In water molecules, the O—H bond length and H—O—H bond angle

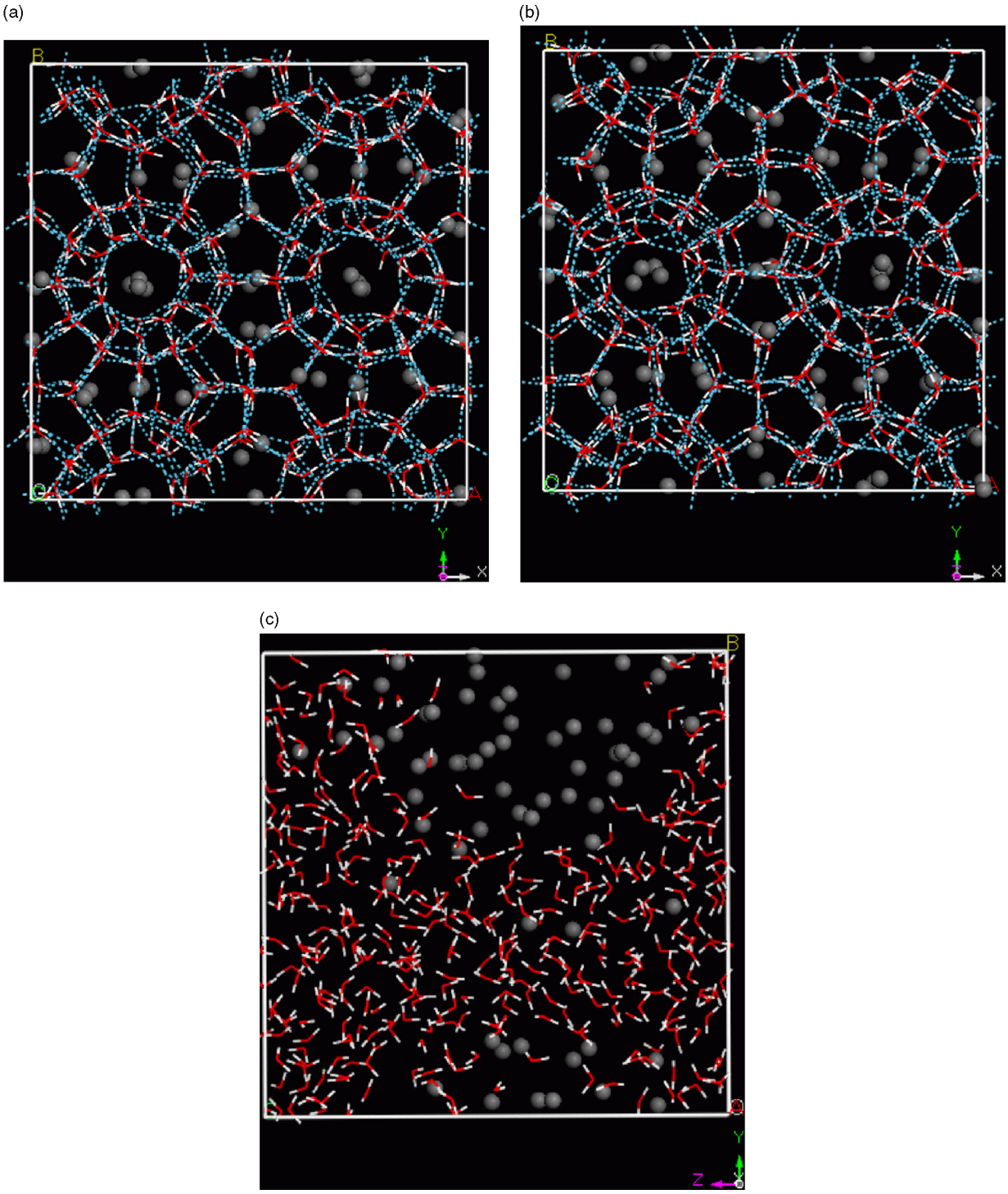

Figure 4. Snapshots of the final configuration at (a) $T = 315$ K, (b) $T = 320$ K and (c) $T = 325$ K.

are constrained at 1.00 Å and at 109.47°, respectively. There are three charges on every water molecule, two of magnitude $+0.41e$ located on each hydrogen atom and one of magnitude $-0.82e$ on oxygen atom.

For simplicity and to minimize the computational efforts, methane molecules are treated as spherical particles, and Lennard–Jones potentials are used for methane–methane interactions according to the OPLS parameterization [20]. The Lennard–Jones parameters of water and methane molecules used in this work are listed in table 1.

The standard Lorentz-Berthelot combining rule is adopted for the methane–water nonelectrostatic interactions.

NPT MD simulations are performed with periodic boundary conditions using DL_POLY MD software package [21] at pressure $P = 30$ bar and temperatures $T = 315$, 320 and 325 K, respectively. Long-ranged electrostatic interactions are handled by the Ewald summation method, and nonelectrostatic interactions are truncated at a distance of 11 Å.

The total simulation time is 500 ps with time step 1 fs and 150 ps for equilibration at each temperature. The equations of motion are integrated using the Leapfrog algorithm. The rigid water molecule constraints are implemented using Shake algorithm with periodic velocity rescaling to maintain the required average temperature of the system.

3. Results and discussions

3.1 Snapshots and mean square displacements (MSD)

In order to give the general features of the system configuration, snapshots of the final configurations of methane hydrate at temperatures of 315, 320 and 325 K are shown in figure 4. Figure 4 shows that the crystalline structure of methane hydrate kept stable when $T \leq 320$ K. The collapse of hydrate structure will be observed, and methane molecules will evidently aggregate together at 325 K.

The MSD of water and methane molecules as a function of time interval t' from 0 to 400 ps at 315, 320 and 325 K are presented in figure 5, respectively. MSD is a measure of the average distance a molecule travels over some time interval, defined as

$$R(t') = \langle \Delta^2 r(t') \rangle = \frac{1}{N} \sum_{i=1}^{N} \left\langle [R_i(t_0 + t') - R_i(t_0)]^2 \right\rangle, \quad (2)$$

where, t_0 is the reference time, $R(t')$ is the MSD, $R_i(t_0)$ is the position of molecule i in the system at run time t_0, where the summation is over all the finite system containing N identical molecules. The angular bracket indicates an average over many such reference times. For a stable crystal, the constituent molecules will vibrate around their lattice sites without diffusing. Such behaviour will be indicated by the appearance of a plateau in the MSD, with the height of this plateau reflecting the final displacements.

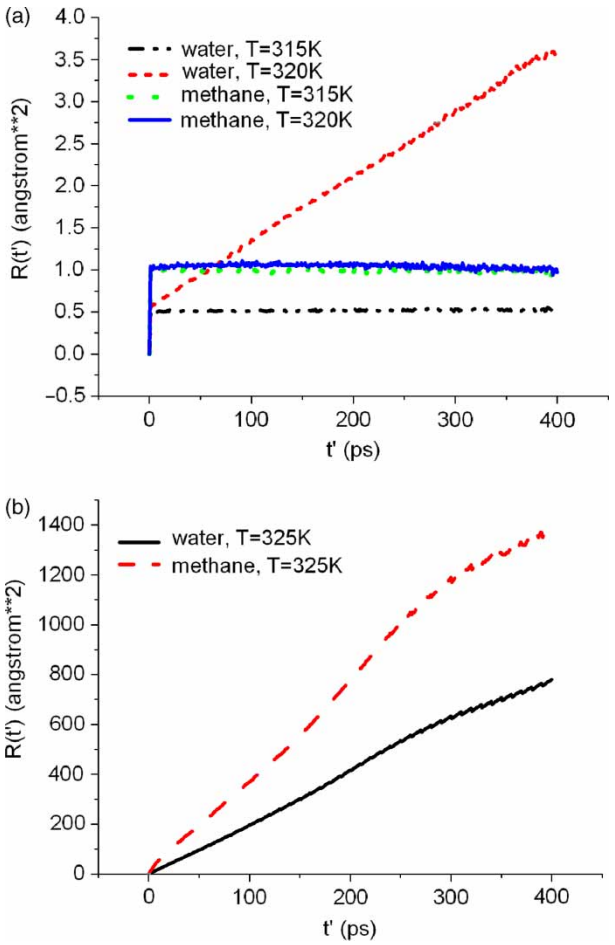

Figure 5. MSDs of water and methane molecules at (a) $T = 315$, 320 K and (b) $T = 325$ K.

Figure 5 indicates that at relatively low temperature $T = 315$ K, the MSD profile of water molecules is typical of stable crystal with a plateau of about 0.5 Å^2, indicating lattice vibrations with amplitudes of about 0.7 Å. At the intermediate temperature $T = 320$ K, it is interesting to note that the MSD of water molecules is slightly diffusing, although the hydrate is still solid-like, as is shown in the snapshot of figure 4. However, there is no analogous diffusive behaviour found in the MSD of methane molecules at $T = 320$ K, which, on the contrary, shows a typical feature of crystalline solid. When the temperature reaches 325 K, the MSD profiles of water and methane molecules are both evidently diffusive, showing evidences of crystal corruption.

Perhaps the most striking feature of figure 5 is the variations in the behaviour of MSD for water and methane molecules at 320 K. In particular, water molecules present a trend of diffusion, while this is not exhibited at all in the MSD for methane molecules. Considering that some extent of crystal distortion is observed in figure 4(b), it could be concluded that the diffusive behaviour of water molecules only results in some extent of crystal distortion. The vibration of water molecules is strong enough to lead

Table 2. Diffusion coefficients of water and methane at different temperatures.

T (K)	H_2O ($cm^2\,s^{-1}$)	CH_4 ($cm^2\,s^{-1}$)
315	0.2×10^{-7}	0.1×10^{-7}
320	1.7×10^{-7}	0.1×10^{-7}
325	3.3×10^{-5}	8.7×10^{-5}

the increasing excursions of equilibrium positions to their lattice sites. The crystal lattice of methane hydrate could be considered metastable. Nevertheless, melting would be observed if the simulation was continued for a sufficiently long time. Therefore, it is reasonable to conjecture that the

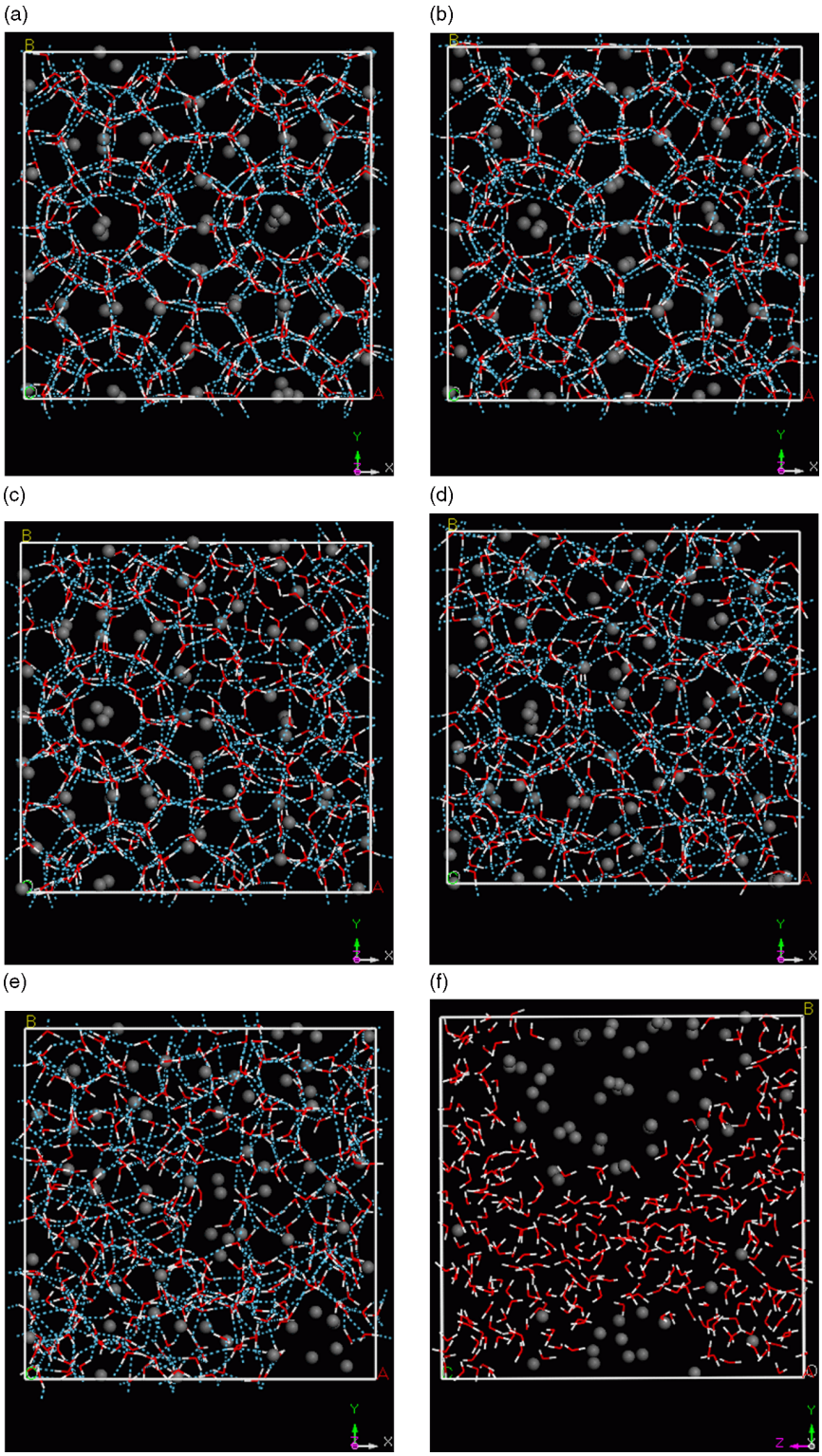

Figure 6. Snapshots of the dissociation process of methane hydrate at 325 K for (a) $t = 100$ ps, (b) $t = 160$ ps, (c) $t = 180$ ps, (d) $t = 190$ ps, (e) $t = 200$ ps and (f) $t = 250$ ps.

original stage of hydrate dissociation is associated with the diffusion of host molecules from their lattice sites.

The diffusion coefficient provides a different measure of the extent to which the system structure is crystalline. It can be obtained from the Einstein relation

$$6Dt' = \langle R(t')^2 \rangle, \tag{3}$$

where D is the diffusion coefficient, $R(t')$ is the MSD within the time interval t'. The calculated diffusion coefficients of water and methane molecules at 315, 320 and 325 K are presented in table 2. Apparently, the diffusion coefficient of methane molecules is much lower than that of water molecules when $T \leq 320$ K, while at 325 K the situation is completely different, implying the methane molecules escape from lattice cavities and hydrate dissociation occurred. That is to say, the diffusion coefficient of methane has been much higher than that of water. According to the present simulation studies, this can be used as a distinct feature to judge whether the hydrate dissociated or not, which will be further illustrated later in this paper.

To further investigate the dissociation process in details, the snapshots of configurations of methane hydrate at 325 K are shown in figure 6 in the sequence of run time t. At $t = 100$ ps, the configuration is an evidently regular hydrogen-bonded network. The simulation system remains strongly crystalline when $t \leq 160$ ps, although some degree of crystal distortion can be observed. At $t = 180$ ps, the crystal distortion becomes more pronounced. There is evidently some degradation of hydrate structure, but most of the cavities still keep stable. A significant loss of the crystalline structure can be observed at $t = 190$ ps. The hydrate structure is completely destroyed and become liquid-like at $t = 200$ ps. A few of the methane molecules even aggregate together, but most of the methane molecules are still dissolved in water. At $t = 250$ ps, a phase separation process can evidently be observed, in which most of the methane molecules aggregated together. The melting process of methane hydrate can be fully presented in figure 6 from $t = 160$ to 200 ps.

Figure 7 depicts the MSD of water and methane molecules from $t = 160$, 170 and 180 ps at 325 K. At $t = 160$ ps, the MSD of methane molecules is typical of crystalline structure, while the MSD of water molecules indicates the water molecules vibrating with a higher amplitude, implying slightly diffusive. The behaviour of water molecules can be regarded as an evidence of pre-melting, which is the first signal before crystal collapse. At $t = 170$ ps or more, water and methane molecules will perform diffusive.

Figure 8 displays the diffusion coefficients of water and methane molecules from $t = 160$ to 200 ps at 325 K. The diffusion coefficient of methane molecules is lower than that of water molecules when $t \leq 190$ ps. However, the diffusion coefficient of methane molecules is much higher than that of water molecules at $t = 200$ ps. Therefore, it can conclude that the hydrate will dissociate when

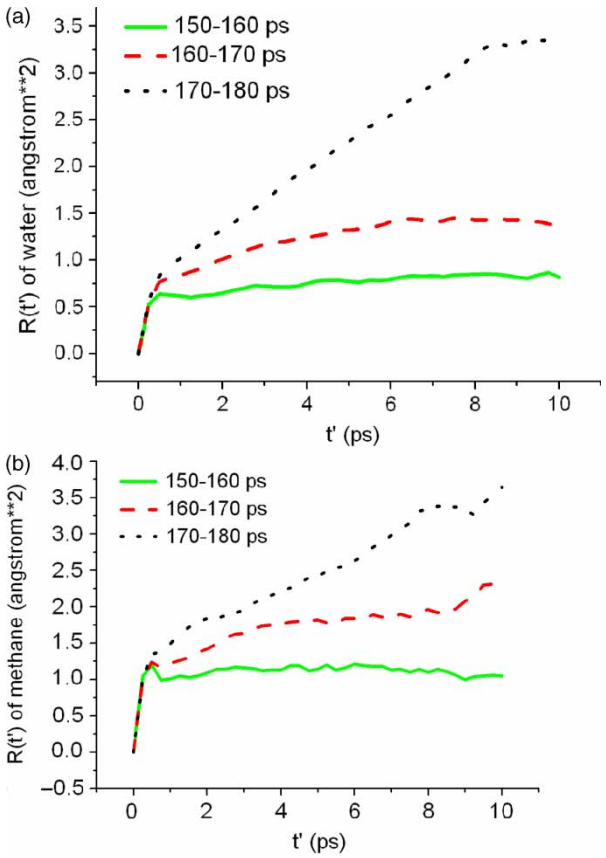

Figure 7. MSDs of (a) water and (b) methane molecules at 325 K and run time $t = 160$, 170 and 180 ps.

$t > 190$ ps. These results are in accord with the conclusions drawn from figure 6, with better resolution. Moreover, these results have reinforced the conclusion drawn from table 2.

3.2 Cell size

The change on the average cell size at run time from $t = 160$ to 200 ps is shown in figure 9. The cell size increases gradually and linearly with the increasing run time when $t \leq 180$ ps. Considering that the MSD of water

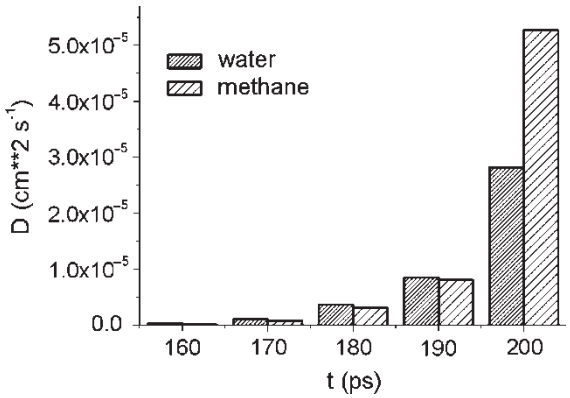

Figure 8. Diffusion coefficients of water and methane at 325 K and run time $t = 160$, 170, 180, 190 and 200 ps.

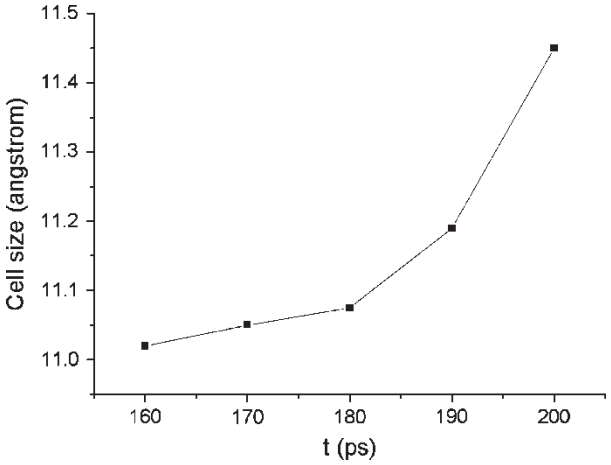

Figure 9. Cell Size vs. run time.

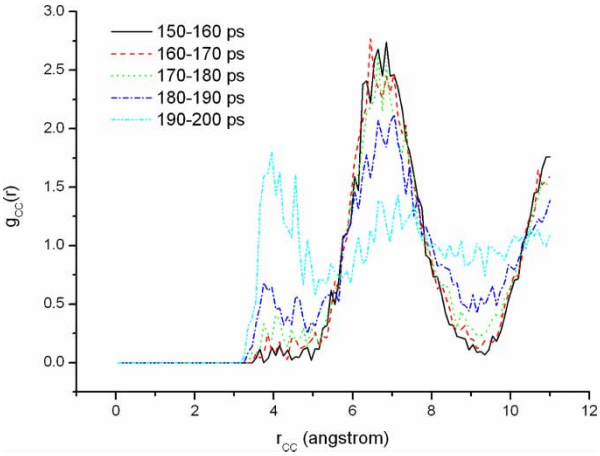

Figure 11. The RDF of carbon atoms at different run time.

molecules become diffusive as early as $t = 160$ ps, the vibration amplitude of the host molecules will be gradually higher with increasing run time, which in turn will result in a much looser crystal structure and more severe crystal distortion. The increase of cell size will become somewhat slope at $t = 190$ ps, indicating the crystal distortion is too severe to maintain the crystal structure stable. A more dramatic change on the cell size at $t = 200$ ps than that at $t = 190$ ps will occur, because the crystal structure has been broken completely.

3.3 Radial distribution function (RDF)

To further establish the structure of methane hydrate at 325 K, figure 10 presents the RDF of oxygen atoms $g_{oo}(r)$ in water molecules when run time $t = 160$, 170, 180, 190 and 200 ps. RDF is defined as the probability of finding a pair of particles at a distance r apart, relative to the probability expected for a completely random distribution at the same density. The first distinct peak represents the distribution of the neighbouring particles. The RDF curves of run time $t = 160$, 170, 180 and 190 ps show two peaks at almost the same locations. The first maximum peak in $g_{oo}(r)$ is located at 2.78 Å, and hence it is known that the nearest oxygen atoms are separated from each other at a distance of around 2.78 Å. It can be therefore inferred the hydrogen bond length is about 1.8 Å. The second

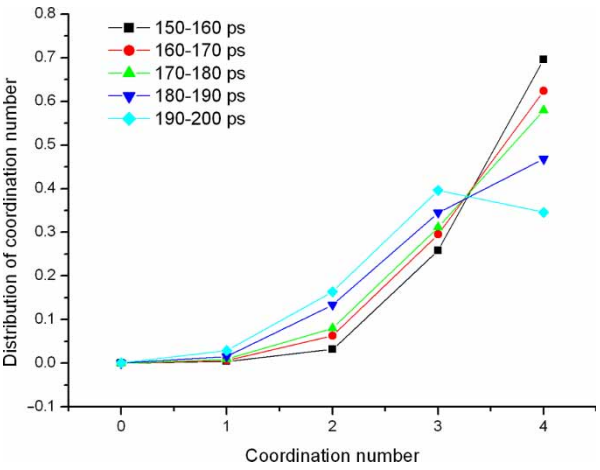

Figure 12. The distribution of coordination numbers of water molecules at different run time.

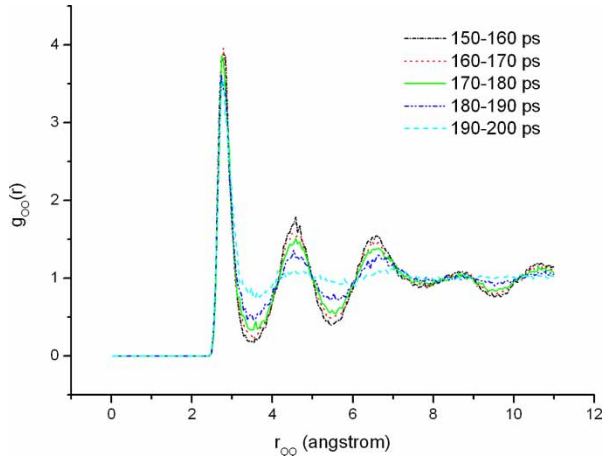

Figure 10. The RDF of oxygen atoms at different run time.

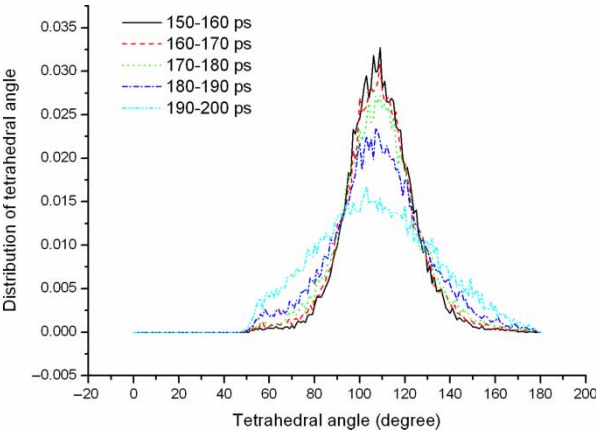

Figure 13. The distribution of tetrahedral angles of water molecules at different run time.

maximum peak appears at a separation of about 4.53 Å, which indicates the existence of tetrahedral hydrogen bonding structures of water molecules in methane hydrate. As run time increases from 160 to 180 ps, the changes in $g_{oo}(r)$ are confined to slight reductions in peak heights and increases in peak widths, indicating a continuously slight crystal degradation due to the loosing and crystal distortion of hydrate structure. The changes in peak heights and peak widths are much more pronounced as $t = 190$ ps, some of the crystal cavities start to break.

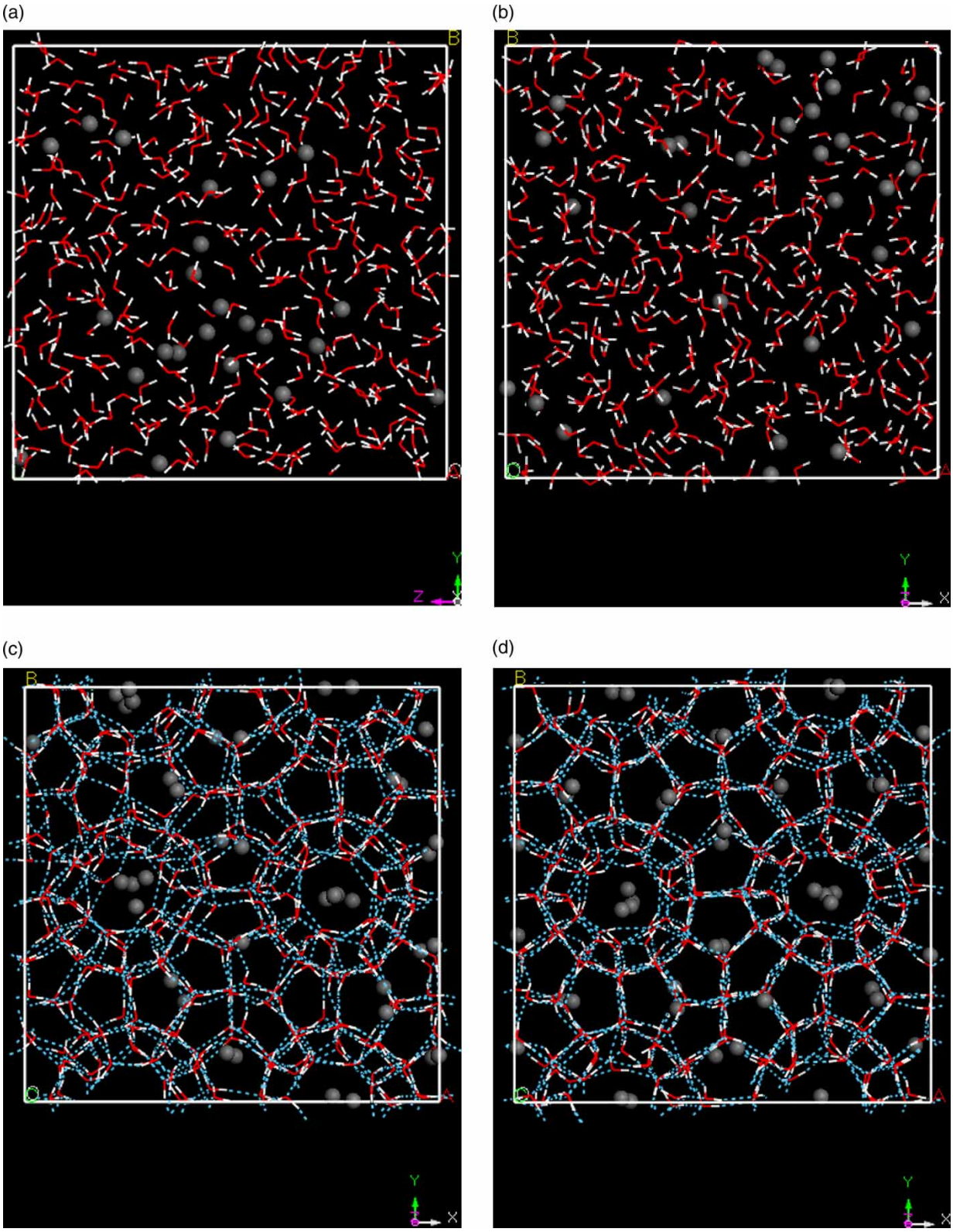

Figure 14. Snapshots of the final configuration when (a) $\theta = 0.375$, (b) $\theta = 0.5$, (c) $\theta = 0.625$ and (d) $\theta = 0.75$.

As $t = 200$ ps, the second maximum peak is almost horizontal, indicating a complete destruction of methane hydrates.

Figure 11 displays the RDF of carbon atoms $g_{cc}(r)$ in methane molecules at 325 K as run time $t = 160$, 170, 180, 190 and 200 ps. It can be inferred that the methane atoms are separated from each other at a distance of about 6.6 Å. When run time $t \geq 190$ ps, a distinct peak at 4 Å appears, indicating that the melting process is associated with the aggregation of methane gas molecules once crystal cavities broken.

3.4 Coordination number and tetrahedral angle

Figure 12 illustrates the distribution of hydrogen bond coordination number of water molecules, for investigating the hydrogen-bonded network during methane hydrate dissociation. When the run time increases from $t = 160$ to 180 ps, most of the water molecules still participate in the tetrahedral hydrogen-bonded network, even the percentage of 4-coordinated water molecules exhibits somewhat reduction. The percentage of 4-coordinated water molecules will appreciably further decrease at $t = 190$ ps. The 3-coordinated water molecules will become dominant at $t = 200$ ps, indicating that the tetrahedral hydrogen-bonded network is no longer the major form among water molecules after the melting of hydrate.

As shown in figure 12, each water molecule will hydrogen-bond to 4 water molecules in a stable hydrate and form a tetrahedral hydrogen-bonded network structure. The tetrahedral angles of water molecules can be seen as a final probe of the hydrogen-bonded network.

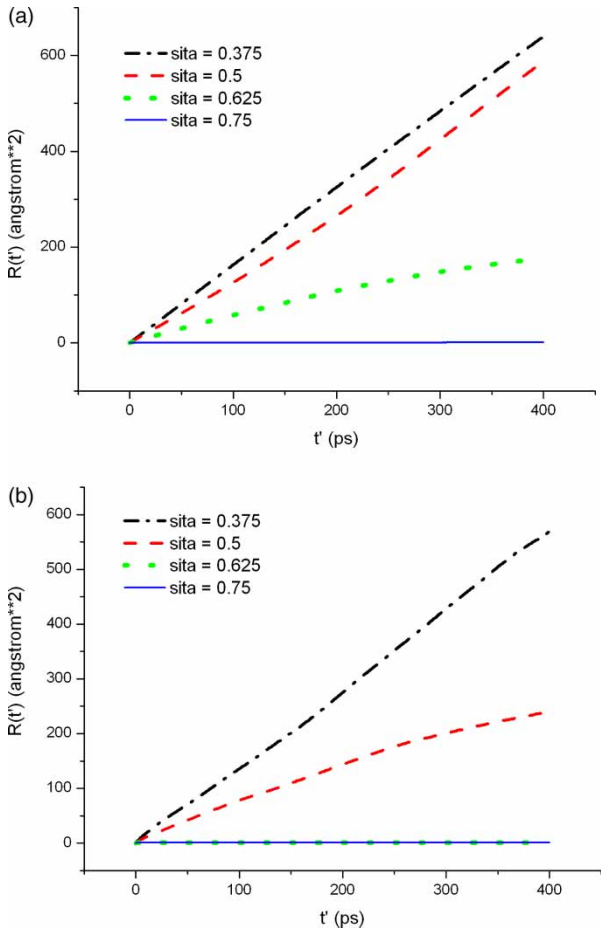

Figure 15. MSDs of (a) water and (b) methane molecules when $\theta = 0.375$, 0.5, 0.625 and 0.75.

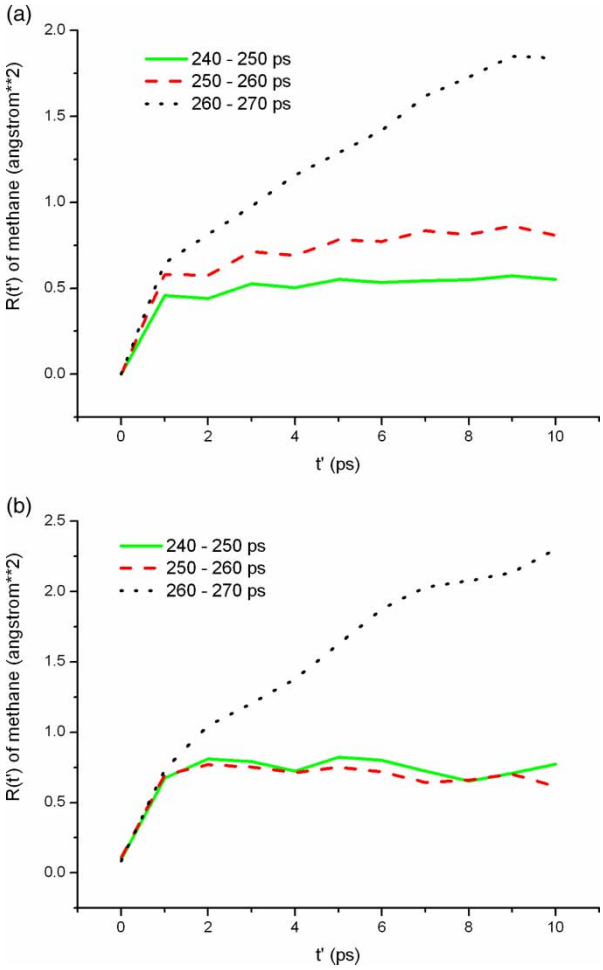

Figure 16. MSDs of (a) water and (b) methane molecules when $\theta = 0.375$ and run time $t = 250$, 260 and 270 ps.

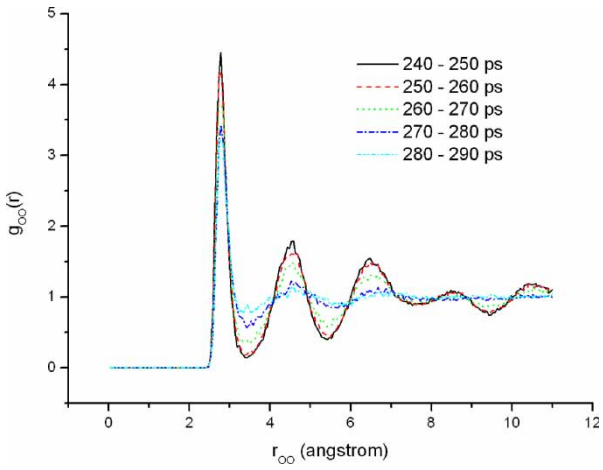

Figure 17. The RDF of oxygen atoms at different run time when $\theta = 0.375$.

The tetrahedral angle θ of a water molecule is thus defined as the average bond angle formed by the central oxygen atom with pairs of oxygen atoms from among its hydrogen-bonded water molecules. For a perfect tetrahedral structure, the tetrahedral angle equals to 109.47°. The calculated distribution of tetrahedral angles for water molecules are presented in figure 13. There is an evident peak located at about 109.47° when run time $t = 160$ ps, indicating a nearly perfect tetrahedral structure. The peak will gradually weaken and broaden with run time increasing. The changes in peak height and peak width is pronounced when $t \geq 190$ ps. It is interesting to note that a peak located at about 109.47° still remains even at $t = 200$ ps, indicating that there are still some tetrahedral structures remaining in the liquid phase.

In this paper, all the MD calculations are based on the assumption of full occupancy of each cage by methane molecule. Actually, it can occur more easily in nature if one or more of the cages are empty. In that case, we might expect that methane molecules could move more easily between cages leading to a very different behaviour. To investigate whether this could be the case, we have also performed a series of MD simulations for different degrees of cage occupancy at $p = 30$ bar. Considering that the stability ability of methane hydrate will decrease with decreasing cage occupancy, these MD simulations have been carried out at a lower temperature $T = 290$ K in order to investigate the gradual dissociation processes of partly-occupied methane hydrates. As a result, we observed substantially similar dissociation behaviour.

Figure 14 presents the snapshots of the final configurations of methane hydrate when cage occupancy $\theta = 0.375$, 0.5, 0.625 and 0.75. Figure 15 shows the MSD of water and methane molecules as a function of time interval t' when cage occupancy $\theta = 0.375$, 0.5, 0.625 and 0.75, respectively. It can be seen from figure 15 that when cage occupancy $\theta = 0.75$, the MSD profiles of water and methane molecules are both typical of stable crystal. When cage occupancy $\theta \leq 0.5$, the MSD profiles of water and methane molecules are both evidently diffusive, showing evidences of crystal corruption. When cage occupancy $\theta = 0.625$, the MSD of water molecules is slightly diffusing. However, the MSD of methane molecules does not present a trend of diffusion, indicating that the hydrate is metastable, as is shown in the snapshot of figure 14.

Figure 16 presents the MSD of water and methane molecules when cage occupancy $\theta = 0.375$ and run time $t = 250$, 260 and 270 ps, respectively. At $t = 250$ and 260 ps, the MSD profiles of methane molecules are typical of crystalline structure, while the MSDs of water molecules are slightly diffusive. At $t = 270$ ps, both water and methane molecules perform diffusive.

Figure 17 presents the RDF of oxygen atoms $g_{oo}(r)$ in water molecules when cage occupancy $\theta = 0.375$ from run time $t = 250$ to 290 ps. It can be seen from figure 17 that as run time increases from 250 to 270 ps, the changes in $g_{oo}(r)$ are confined to slight reductions in peak heights and increases in peak widths, indicating a continuously slight crystal degradation due to the loosing and crystal distortion of hydrate structure. The changes in peak heights and peak widths are much more pronounced when $t \geq 280$ ps, and the second maximum peak is almost horizontal, indicating the crystal distortion is too severe to maintain the crystal structure stable. Figure 18 presents the RDF of carbon atoms $g_{cc}(r)$ in methane molecules when cage occupancy $\theta = 0.375$ from run time $t = 250$ to 290 ps. It is apparent that the aggregation of methane molecules is observed when $t \geq 280$ ps.

Figure 19 gives the snapshots of the final configurations of methane hydrate from run time $t = 250$ to 290 ps when cage occupancy $\theta = 0.375$. It can be seen that no methane molecules were observed to travel between cages up to $t = 270$ ps, when the crystal lattices were relatively stable. A few methane molecules began to escape from their original cages and move between cages at $t = 280$ ps, while the lattice crystals were almost hard to discriminate. More detailed description about these simulation results will be published elsewhere [22].

4. Conclusions

The MD simulations are performed on the dissociation process of methane hydrates in this paper at $P = 30$ bar and $T = 315$, 320 and 325 K. A series of analytical results concerned with the dissociation process, MSD and diffusion coefficients of water and methane molecules, RDF of O atoms in water molecules and C atoms in methane molecules, cell size and coordination number and tetrahedral angle of water molecules in hydrates, are presented, from which a general picture of the dissociation process of methane hydrate can be drawn.

At the very beginning of hydrate dissociation, the crystal distortion is associated with the diffusive behaviour of host molecules. With the progress of dissociation, a continuous increase will be observed in the vibrational amplitude of host molecules, and the cell size and crystal

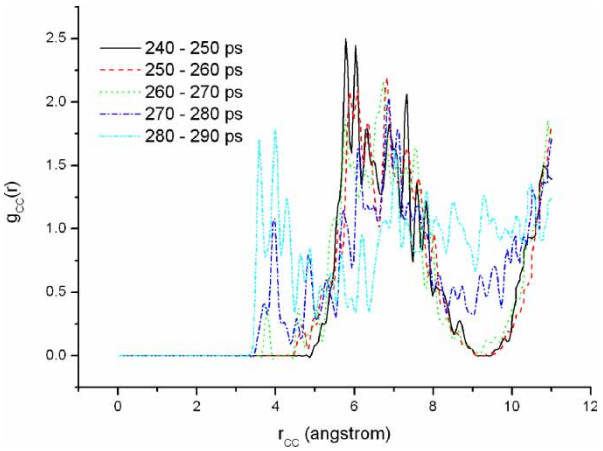

Figure 18. The RDF of carbon atoms at different run time when $\theta = 0.375$.

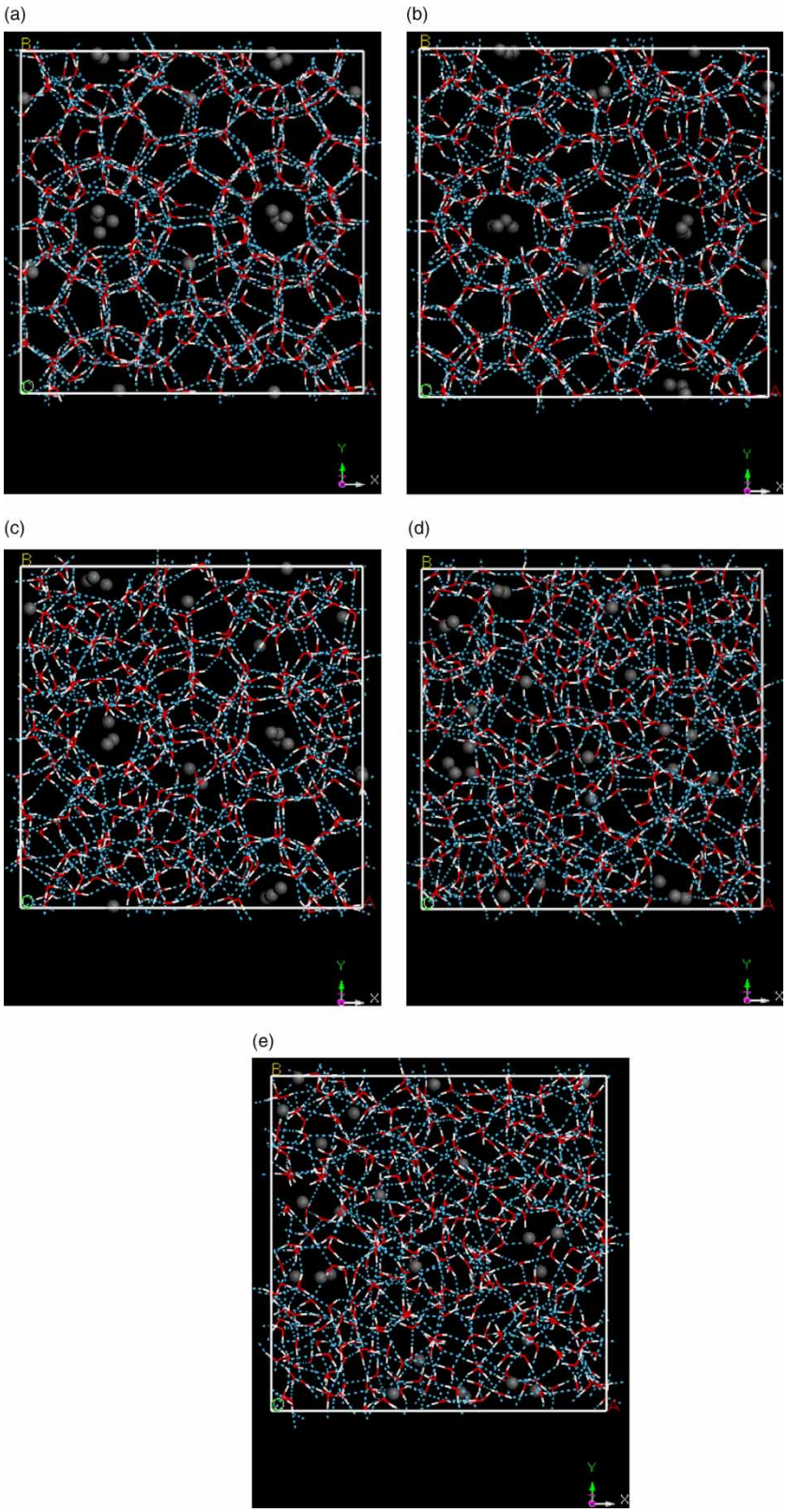

Figure 19. Snapshot of the dissociation process of methane hydrate when $\theta = 0.375$ for (a) $t = 250$ ps, (b) $t = 260$ ps, (c) $t = 270$ ps, (d) $t = 280$ ps and (e) $t = 290$ ps.

distortion will increases gradually. This in turn will result in a higher vibrational amplitude of both host and guest molecules. The hydrate cavities will start to break as the crystal distortion is too severe to maintain the lattice structure. The guest molecules will escape quickly from the lattice structure and gradually aggregate together once the crystal cavities destroyed. It is interesting to note that the dynamical transition in host molecules occurs

earlier than that in guest molecules. In addition, the diffusion coefficient of methane molecules is substantially lower than that of water molecules in a stable methane hydrate, which can be used to determine whether the hydrate has been dissociated or not. No methane molecules are observed to travel between cages when the crystal lattices are relatively stable. It is also interesting to observe that there are some tetrahedral hydrogen-bonded network still remaining in the liquid phase even the hydrate is fully dissociated, but 3-coordinated water molecules become the dominant.

The dissociation of methane hydrate is considered to be comprised of two stages. The first stage is the process associated with the diffusive behaviour of host molecules, which gradually leads to the increase of the cell size and ultimately results in the fracture of the lattice structure. The second stage is such a process in which methane molecules will escape from the broken hydrate cavities and aggregate together. The fracture of the lattice structure is found to be the key for hydrate dissociation. These descriptions are substantially in accord with the two-step dissociation mechanism proposed by Sloan [23].

Acknowledgements

This work is financially supported by the National Natural Science Foundation of China under Grant No. 20221603. We gratefully acknowledge Professor W. Smith of CCLRC Darebury Laboratory and Professor P. Mark Rodger of University of Warwick for their valuable discussions. Also, we acknowledge the Virtual Laboratory of Computational Chemistry, Computer Network Information Centre, Chinese Academy of Sciences, for the use of its resources.

References

[1] E.D. Sloan. *Clathrate Hydrates of Natural Gases*, Marcel Dekker Inc., New York (1990).
[2] E.G. Hammerschmidt. Formation of gas hydrate in natural gas transmission lines. *Ind. Eng. Chem.*, **26**, 851 (1934).
[3] K.A. Kvenvolden. Potential effects of gas hydrate on human welfare. *Proc. Natl. Acad. Sci. USA*, **96**, 3420 (1999).
[4] J.S. Gudmundsson, A.A. Khokhar, M. Parlaktuna. Storing natural gas as frozen hydrate. *SPE Prod. Facil.*, **9**, 69 (1994).
[5] J.S. Gudmundsson. Natural gas hydrate—an alternative to liquefied natural gas? *Pet. Rev.*, **50**, 232 (1996).
[6] J.S. Gudmundsson. Hydrates for deep ocean storage of Co_2, paper presented at Proceedings of the Fifth International Conference on Gas Hydrates, Trondheim (2005).
[7] E.D. Sloan. Clathrate hydrates: The other common solid water phase. *Ind. Eng. Chem. Res.*, **39**, 3123 (2000).
[8] C.A. Koh. Towards a fundamental understanding of natural gas hydrates. *Chem. Soc. Rev.*, **31**, 157 (2002).
[9] P.R. Bishnoi, V. Natarajan. Formation and decomposition of gas hydrates. *Fluid Phase Equilib.*, **117**, 168 (1996).
[10] H.C. Kim, P.R. Bishnoi. H. R. A. Kinetics of methane hydrate decomposition. *Chem. Eng. Sci.*, **42**, 1645 (1987).
[11] M. Ota, Y. Qi. Numerical simulation of nucleation process of clathrate hydrates. *JSME Int. J.*, **43**, 719 (2000).
[12] C. Moon, P.C. Taylor, P.M. Rodger. Molecular dynamics study of gas hydrate formation. *J. Am. Chem. Soc.*, **125**, 4706 (2003).
[13] M.T. Kirchner, R. Boese, W.E. Billups, L.R. Norman. Gas hydrate single-crystal structure analyses. *J. Am. Chem. Soc.*, **126**, 9407 (2004).
[14] J.D. Bernal, R.H. Fowler. A theory of water and ionic solution, with particular reference to hydrogen and hydroxy ions. *J. Chem. Phys.*, **1**, 515 (1933).
[15] J.S. Tse, M.L. Klein, I.R. McDonald. Molecular dynamics studies of ice ic and structure I clathrate hydrate of methane. *J. Phys. Chem.*, **87**, 4198 (1983).
[16] J.S. Tse, M.L. Klein, I.R. McDonald. Computer simulation studies of the structure I clathrate hydrates of methane, tetrafluoromethane, cyclopropane, and ethylene oxide. *J. Chem. Phys.*, **81**, 6146 (1984).
[17] A.A. Chialvo, M. Houssa, P.T. Cummings. Molecular dynamics study of the structure and thermophysical properties of model Si clathrate hydrates. *J. Phys. Chem. B.*, **106**, 442 (2002).
[18] N.J. English, J.M.D. Macelroy. Structural and dynamical properties of methane clathrate hydrates. *J. Comput. Chem.*, **24**, 1569 (2003).
[19] H.J.C. Berendsen, J.P.M. Postma, W.F. van Gunsteren, J. Hermans. Interaction Models for Water in Relation to Protein Hydration, paper presented at Intermolecular Forces: Proceedings of the Fourteenth Jerusalem Symposium on Quantum Chemistry and Biochemistry, Jerusalem (1981).
[20] W.L. Jorgensen, J.D. Madura, C.J. Swenson. Optimized intermolecular potential functions for liquid hydrocarbons. *J. Am. Chem. Soc.*, **106**, 6638 (1984).
[21] P.M. Rodger, T.R. Forester, W. Smith. Simulations of the methane hydrate/methane gas interface near hydrate forming conditions. *Fluid Phase Equilib.*, **116**, 326 (1996).
[22] L.Y. Ding, C.Y. Geng, Y.H. Zhao, X.F. He, H. Wen. Molecular dynamics simulation on the stability of structure I methane hydrates. *Comput. Appl. Chem.*, **24**, 569 (2007).
[23] A. Gupta, S.F. Dec, C.A. Koh, E.D. Sloan, NMR and Raman Investigations of the methane hydrate dissociation mechanism, paper presented at Proceedings of the Fifth International Conference on Gas Hydrates, Trondheim (2005)